Coupled Microstrip Lines on a Cylindrical Substrate

AKIFUMI NAKATANI, STUDENT MEMBER, IEEE, AND
NICÓLAOS G. ALEXÓPOULOS, FELLOW, IEEE

Abstract — **The characterization of quasi-static and frequency-dependent coupled microstrip lines on a cylindrical substrate is presented in this article. The dyadic Green's function is involved for the full-wave analysis, and the dispersive properties are determined by solving a pair of coupled Fourier summation equations with the Galerkin method. It is shown that the transverse current component effect becomes significant when the odd mode is characterized. Careful numerical treatment reveals the transverse current behavior when the lines are tightly coupled.**

I. Introduction

IN MANY PRACTICAL applications, microstrip antennas and microstrip arrays are conformal to cylindrically shaped substrates [1]–[6]. This has brought about the need for developing accurate frequency-dependent models and computer-aided design tools for microstrip integrated circuits on curved substrates. In a recent article, the dispersive waveguiding properties of an infinitely long, axially oriented microstrip line were characterized [6]. Therein a highly accurate algorithm was described for narrow single microstrip lines; i.e., only the longitudinal current was included in the analysis. This paper investigates the transverse current (transverse field) effect on single as well as coupled microstrip lines. The quasi-static formulation and numerical results are also presented for comparison with the low-frequency limit of the dynamic models. It is determined that the odd mode requires appropriate modeling of the transverse electric field to achieve precise characterization of the coupled microstrip lines. A closed-form formulation is also presented which allows the accurate computation of Galerkin's matrix elements. The geometry of interest is shown in Fig. 1. A curvilinear coefficient R is introduced as the ratio of inner to outer radii, namely $R = a/b$. A local geometry is also defined to show the corresponding dimensions conventionally used for planar geometries. Throughout the paper, the local dimensions and the curvilinear coefficient R are used to define the microstrip line physical characteristics.

Manuscript received April 7, 1987; revised August 7, 1987. This work was supported in part by the National Science Foundation under Grant ECS 86 04837 and in part by Northrop IR&D under Contract HHH107578.

The authors are with the Electrical Engineering Department, University of California, Los Angeles, CA 90024.

IEEE Log Number 8717247.

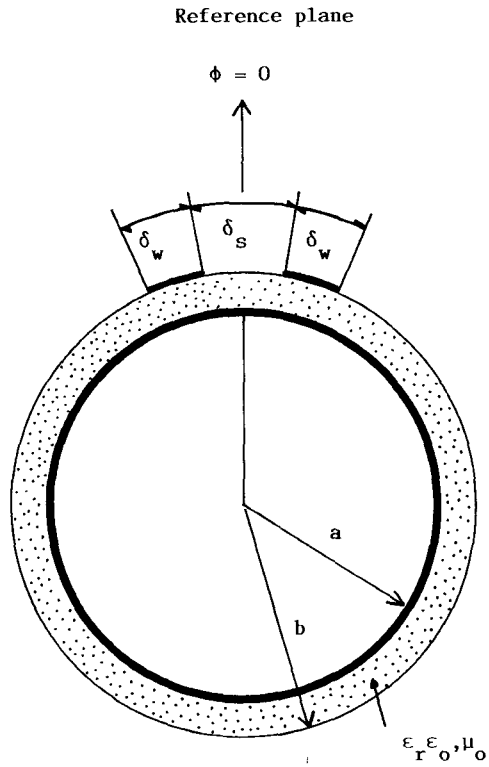

Fig. 1. Coupled microstrip lines on cylindrical substrate. R: curvilinear coefficient = a/b. $W = \delta_w b$, $s = \delta_s b$, and $h = b - a$.

II. Analysis

The Green's function approach and the numerical solution of the pertinent Fourier domain analysis permit us to treat a variety of problems by developing the proper form of charge or current distribution [1]–[12] on single or coupled microstrip lines. The potential Green's function is used for the quasi-static while the dyadic Green's function is used for the frequency-dependent formulation. The quasi-static Green's function solution is given in the Appendix. There is an essential difference between the two formulations in that the quasi-static approach relies on the radial field dependence, while the electric dyadic Green's function solution relies on the substrate surface electric field and current. Therefore when coupled lines are considered, the transverse electric field is no longer negligible, since the field strength of the odd mode between the two lines becomes strong enough to compensate for the

0018-9480/87/1200-1392$01.00 ©1987 IEEE

weak transverse current when the separation of the lines becomes small. This necessitates the development of a full-wave analysis. The problem is characterized by considering a magnetic or electric wall at the center of the two strips for the even- and odd-mode analyses, respectively. The microstrip line current density generates an electric field given by

$$\bar{E}(\phi) = \sum_{m=-\infty}^{\infty} \bar{\bar{G}}(m) \cdot \tilde{\bar{J}}(m) \exp(jm\phi) \tag{1}$$

where $\bar{\bar{G}}(m)$ denotes the dyadic Green's function and $\sim$ denotes the Fourier transform of the quantity of interest. In (1), $\tilde{\bar{J}}(m)$, $\bar{E}(\phi)$, and $\bar{\bar{G}}(m)$ are defined as

$$\tilde{\bar{J}}(m) = \hat{t}\tilde{J}_t(m) + \hat{z}\tilde{J}_z(m) \tag{2}$$

$$\bar{E}(\phi) = \hat{t}E_t(\phi) + \hat{z}E_z(\phi) \tag{3}$$

and

$$\bar{\bar{G}}(m) = \begin{pmatrix} G_{tt}(m)\hat{t}\hat{t} & G_{tz}(m)\hat{t}\hat{z} \\ G_{zt}(m)\hat{z}\hat{t} & G_{zz}(m)\hat{z}\hat{z} \end{pmatrix} \tag{4}$$

where t stands for transverse while z represents longitudinal components. The exact form of the dyadic Green's function has been defined previously [1], [3]–[6].

The coupled equations are now solved for the unknown current density $\bar{J}$. When $\bar{J}$ is expanded as

$$\bar{J}(\phi) = \sum_{n=1}^{N} c_n \bar{J}_n(\phi) \tag{5}$$

the substitution of (5) into (1) yields

$$\bar{E}(\phi) = \sum_{n=1}^{N} c_n \left\{ \sum_{m=-\infty}^{\infty} \bar{\bar{G}}(m) \cdot \tilde{\bar{J}}_n(m) \exp(jm\phi) \right\}. \tag{6}$$

When the Galerkin method is applied to (6), a system of equations is obtained in the form

$$[V_{n'}] = [Z_{nn'}][c_n] \tag{7}$$

where the $V_{n'}$ vector and $Z_{nn'}$ matrix elements are defined by

$$V_{n'} = \langle \bar{E}(\phi), \bar{J}_{n'}(\phi) \rangle \tag{8}$$

and

$$Z_{nn'} = \left\langle \sum_{m=-\infty}^{\infty} \bar{\bar{G}}(m) \cdot \tilde{\bar{J}}_n(m) \exp(jm\phi), \bar{J}_{n'}(\phi) \right\rangle. \tag{9}$$

The notation $\langle\ \rangle$ represents the inner product of the functions on the strip segment. Furthermore, the inner product of (9) can be analytically carried out since its inner product is a conjugate Fourier transform operation. Thus, (9) is rewritten as

$$Z_{nn'} = \sum_{m=-\infty}^{\infty} \tilde{\bar{J}}_{n'}^{*}(m) \cdot \bar{\bar{G}}(m) \cdot \tilde{\bar{J}}_n(m). \tag{10}$$

When the infinite line is considered, the inner product of the electric field and current density functions vanishes because of the complementary relationship. Therefore, the properties of the above set of equations can be computed by seeking for the nontrivial solution of the Galerkin determinant. The basis function set must be chosen in order to achieve sufficient convergence of the Fourier summation form as given in (10). The large order behavior of the dyadic Green's function is derived as

$$\lim_{m \to \infty} \bar{\bar{G}}(m) = \begin{pmatrix} mB_{tt}\hat{t}\hat{t} & B_{tz}\hat{t}\hat{z} \\ B_{zt}\hat{z}\hat{t} & B_{zz}/m\hat{z}\hat{z} \end{pmatrix} \tag{11}$$

where

$$B_{tt} = \frac{j\eta}{k_0 b} \frac{1}{1+\epsilon_r} \tag{12a}$$

$$B_{zt} = B_{tz} = \frac{jk_z b\eta}{k_0 b} \frac{1}{1+\epsilon_r} \tag{12b}$$

and

$$B_{zz} = -\frac{jk_0 b\eta}{2}\left(1 - \frac{2\epsilon_{\text{eff}}}{1+\epsilon_r}\right). \tag{12c}$$

The effective dielectric constant ϵ_{eff} is defined by $(k_z/k_0)^2$, where k_z is the wavenumber in the axial direction and η is the free-space characteristic impedance. The choice of current basis functions is important in achieving convergence. This is especially true for the transverse current basis function choice. The numerical precision of the computation depends strongly on the accuracy of each Galerkin determinant element value. The slow convergence of the Fourier summation form when the circuit dimensions are much smaller than the radius of the cylinder has been pointed out previously [5], [6]. This necessitates the development of a closed-form expression in order to avoid the numerical inaccuracy caused by truncating the tail contribution of the summation. This procedure is also important to detect the small contribution of the transverse current since its magnitude is usually 10^{-3} to 10^{-6} relative to the longitudinal component when the frequency is very low. Numerical efficiency is also seriously improved when the closed-form expression is used. It is not necessarily true that numerical efficiency and accuracy are improved by using complicated basis sets with a smaller number of basis functions. Because of the above-mentioned reasons, triangular basis functions have been chosen for the transverse current representation, while pulse basis functions have been used for the longitudinal basis current formulation, as shown in Fig. 2. The Galerkin determinant elements must be properly normalized to avoid numerical overflow or underflow when a large number of basis functions are used. N basis functions are employed for both the longitudinal and the transverse current expansion for one line. The basic Fourier transform of the above

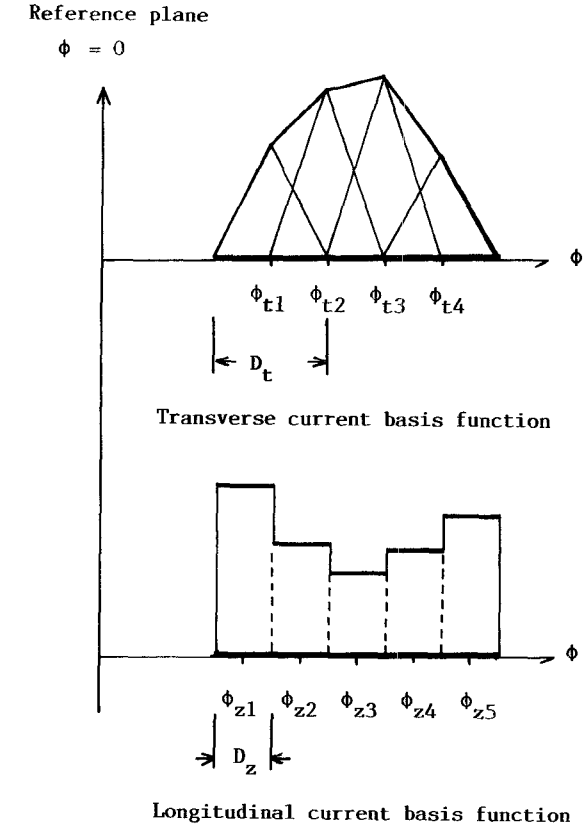

Fig. 2. Current basis functions.

functions is derived as follows:

(a) transverse basis function: $J_{t0}(\phi) = (1 - |2\phi/D_t|)$ where $|\phi| < D_t/2$,

$$\underset{\sim}{J}_{tn}^{(+,-)} = \frac{D_t}{4\pi} \exp\{(-,+)\, jm\phi_{tn}\} \operatorname{sinc}^2\left(\frac{mD_t}{4}\right) \quad (13a)$$

(b) longitudinal basis function: $J_{z0}(\phi) = 1$ where $|\phi| < D_z/2$,

$$\underset{\sim}{J}_{zn}^{(+,-)} = \frac{D_z}{2\pi} \exp\{(-,+)\, jm\phi_{zn}\} \operatorname{sinc}\left(\frac{mD_z}{2}\right) \quad (13b)$$

where D_t and D_z are defined as $2\delta_w/(N+1)$ and δ_w/N, respectively, and the Fourier transform shifting property is applied. The relative position of the basis functions is referenced from the center of the two strips, i.e., $\phi = 0$, and the $+,-$ signs indicate the positive and negative position from the reference plane. The function $\operatorname{sinc}(x)$ is defined as $\sin(x)/x$. The above set of basis functions ensures convergence of the Fourier summation. Furthermore, the Galerkin procedure also equalizes the convergence rate of each matrix element. When even and odd modes are considered, a magnetic or an electric wall is placed at the center of the two strips. Therefore we obtain $J_{tn}^{(e)} = (J_{tn}^{+} - J_{tn}^{-})/2$ and $J_{zn}^{(e)} = (J_{zn}^{+} + J_{zn}^{-})/2$ for the even mode and $J_{tn}^{(o)} = (J_{tn}^{+} + J_{tn}^{-})/2$ and $J_{zn}^{(o)} = (J_{zn}^{+} - J_{zn}^{-})/2$ for the odd mode. The following closed-form expressions are presented for precise and efficient computation of the Fourier summation.

Closed-Form Formulation

The dyadic Green's function components exhibit the following properties: $G_{tt}(m) = G_{tt}(-m)$, $G_{zz}(m) = G_{zz}(-m)$, and $G_{tz}(m) = -G_{tz}(-m)$. Therefore, the Fourier summation reduces to only positive m. This also proves that the previously defined currents are properly chosen, since the choice of even or odd distribution for both transverse and longitudinal currents makes the coupling matrix element zero.

1) Transverse Matrix Element:

$$\bar{X}_{nn'}^{tt} = 2\left(\frac{D_t}{4\pi}\right)^2 \left[\frac{1}{2}(1-p)G_{tt}(0) + B_{tt}\left(\frac{4}{D_t}\right)^4 S_{nn'}^{tt} + \sum_{m=1}^{\infty} \{G_{tt}(m) - mB_{tt}\} \begin{matrix}\sin\\ \cos\end{matrix}(m\phi_{tn'}) \begin{matrix}\sin\\ \cos\end{matrix}(m\phi_{tn}) \cdot \operatorname{sinc}^4\left(\frac{mD_t}{4}\right)\right] \quad (14a)$$

where

$$S_{nn'}^{tt} = \sum_{m=1}^{\infty} \frac{1}{m^3} \begin{matrix}\sin\\ \cos\end{matrix}(m\phi_{tn'}) \begin{matrix}\sin\\ \cos\end{matrix}(m\phi_{tn}) \sin^4\left(\frac{mD_t}{4}\right). \quad (14b)$$

2) Coupling Matrix Element:

$$\bar{X}_{nn'}^{tz} = -\bar{X}_{n'n}^{zt} = -2j(-1)^p \left(\frac{D_t}{4\pi}\right)\left(\frac{D_z}{2\pi}\right)\left[B_{tz}\left(\frac{4}{D_t}\right)^2\left(\frac{2}{D_z}\right) S_{nn'}^{tz} + \sum_{m=1}^{\infty} \{G_{tz}(m) - B_{tz}\} \begin{matrix}\sin\\ \cos\end{matrix}(m\phi_{tn'}) \begin{matrix}\cos\\ \sin\end{matrix}(m\phi_{zn}) \cdot \operatorname{sinc}^2\left(\frac{mD_t}{4}\right)\operatorname{sinc}\left(\frac{mD_z}{2}\right)\right] \quad (15a)$$

where

$$S_{nn'}^{tz} = \sum_{m=1}^{\infty} \frac{1}{m^3} \begin{matrix}\sin\\ \cos\end{matrix}(m\phi_{tn'}) \begin{matrix}\cos\\ \sin\end{matrix}(m\phi_{zn}) \cdot \sin^2\left(\frac{mD_t}{4}\right)\sin\left(\frac{mD_z}{2}\right). \quad (15b)$$

3) Longitudinal Matrix Element:

$$\bar{X}_{nn'}^{zz} = 2\left(\frac{D_z}{2\pi}\right)^2 \left[\frac{1}{2}pG_{zz}(0) + \left(\frac{2}{D_z}\right)^2 B_{zz} S_{nn'}^{zz} + \sum_{m=1}^{\infty} \{G_{zz}(m) - B_{zz}\} \begin{matrix}\cos\\ \sin\end{matrix}(m\phi_{zn'}) \begin{matrix}\cos\\ \sin\end{matrix}(m\phi_{zn}) \cdot \sin^2\left(\frac{mD_z}{2}\right)\right] \quad (16a)$$

where

$$S_{nn'}^{zz} = \sum_{m=1}^{\infty} \frac{1}{m^3} \begin{matrix}\cos\\ \sin\end{matrix}(m\phi_{zn'}) \begin{matrix}\cos\\ \sin\end{matrix}(m\phi_{zn}) \sin^2\left(\frac{mD_z}{2}\right) \quad (16b)$$

and

$$p = \begin{cases} 1: \text{ even mode} \\ 0: \text{ odd mode.} \end{cases}$$

The upper case corresponds to the even while the lower case corresponds to the odd mode. Clausen's integral is applied to construct the summable form of (14b), (15b), and (16b) as described in [13] and [14]. Once the propagation constant of the system is computed, the characteristic impedance can also be obtained by the variational expression developed in [6], i.e.,

$$Z_0 = \frac{2\pi b}{|I_z|^2} \sum_{m=-\infty}^{\infty} J_z(m) V_m J_z^*(m) \tag{17}$$

where V_m is the normalized Fourier-transformed voltage defined between ground and strip as

$$V_m = \int_a^b G_{\rho z}^{(d)}(\rho, m)\, d\rho. \tag{18}$$

The total current I_z is defined on either side of the strip for a coupled line and it has been defined for half of the strip for the single line case. This expression also provides the power relation using the voltage and current definition [12].

III. Numerical Results

The low-frequency results are shown for the alumina substrate case in Figs. 3 and 4. The strip width W and the separation s are defined as $b\delta_w$ and $b\delta_s$, respectively, while the substrate thickness h is defined as $(b-a)$. The effective dielectric constant shows a small variation from the planar geometry, while the characteristic impedance shows much stronger dependence on the substrate curvature parameter. The above data have been also simulated by using the quasi-static formulation, which is provided in the Appendix. The agreement of both approaches is better than 0.2 percent where $k_0 b = 0.1$ is used for the frequency-dependent model. The frequency-dependent single microstrip line is simulated for $R = 0.9$ and $W/h = 1.0$ by taking the numerical limit of $s/h = 0.0$. The even mode is shown in Figs. 5 and 6. The characteristic impedance for the single line defined by (17) must be interpreted properly. The circled data show the longitudinal current approximation [6] (the transverse current has been neglected), while the solid line shows the full-wave current analysis. The transverse current effect can be seen at high frequencies when the microstrip line is wider. The same type of behavior has been predicted in [7] and [8]. The role of the transverse current component effect becomes much clearer when coupled lines are considered.

The next figure shows the low-frequency behavior of coupled microstrip lines by varying s/h (Fig. 7). Here, $R = 0.9$ and $W/h = 1.0$ for an alumina substrate. When the coupled lines are merging to one line, both quasi-static and frequency-dependent solutions predict the appropriate asymptotic behavior for the even- and odd-mode cases. For the even mode, the effective dielectric constant approaches the single line parameter for a line width of $(2W+s)/h$. This is because the even-mode effective line widths overlap before the physical line width comes into contact. The effective dielectric constant in this case tends to increase until the even mode of the coupled microstrip

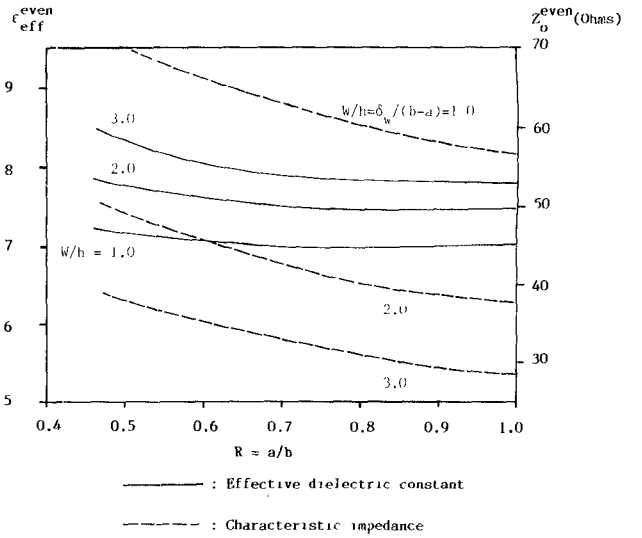

Fig. 3. Low-frequency even-mode microstrip line characteristics. $\epsilon_r = 9.6$ and $s/h = \delta_s b/(b-a) = 1.0$.

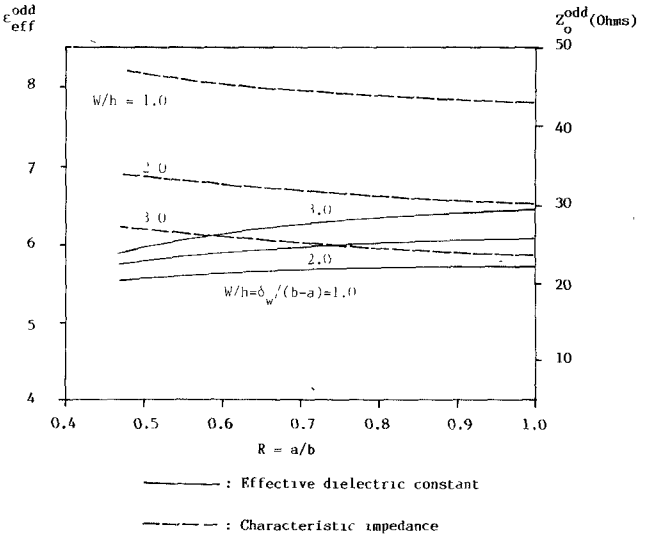

Fig. 4. Low-frequency odd-mode microstrip line characteristics. $\epsilon_r = 9.6$ and $s/h = \delta_s b/(b-a) = 1.0$.

lines sees the actual separation of the line. Thus, for very small separation, the electric field underneath the coupled lines tends to behave as it does for the single line. The odd-mode field, on the other hand, approaches the small slot field distribution behavior as the lines get very close. When the separation becomes extremely small, the effective dielectric constant approaches the value $(\epsilon_r + 1)/2$, in which case the slot field is so strong that the field lines tend to be shared equally in the dielectric and air region. Here the small dashed line indicates the results for the longitudinal current approximation. The longitudinal current approximation for the even mode shows no variation from the full-wave analysis. However the longitudinal current approximation for the odd mode shows a strong discrepancy from both the quasi-static and the full-wave analysis. When the gap is small, the transverse electric field must be taken properly into account in the formulation by using the full-wave analysis. Fig. 8 reveals the odd-mode

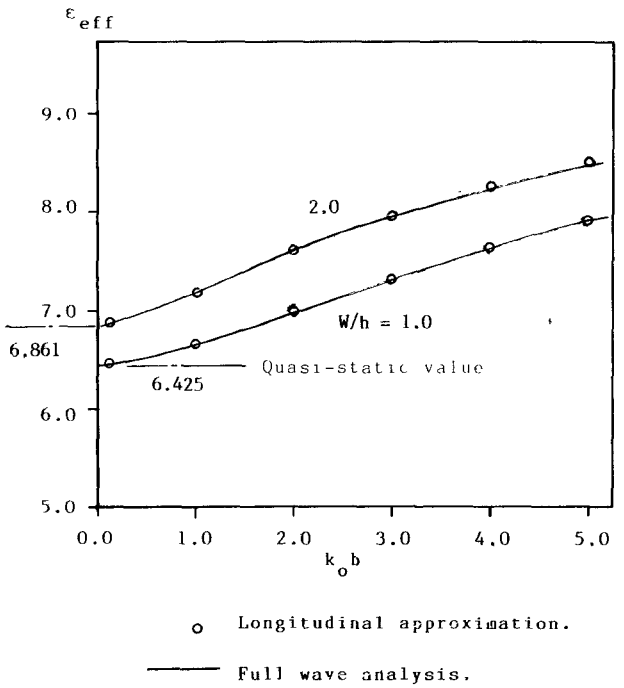

Fig. 5. Frequency-dependent effective dielectric constant of single microstrip line on cylindrical substrate. $R = a/b = 0.9$, $\epsilon_r = 9.6$, and $s/h = \delta_s b/(b-a) = 0.0$.

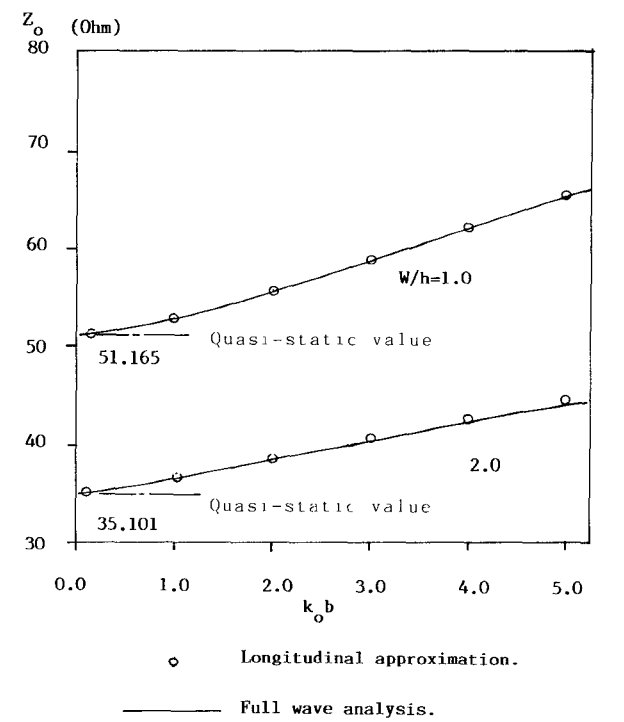

Fig. 6. Frequency-dependent characteristic impedance of single microstrip line on cylindrical substrate $R = a/b = 0.9$, $\epsilon_r = 9.6$, and $s/h = \delta_s b/(b-a) = 0.0$.

current distribution when both longitudinal and transverse currents are included for various line separations. The cylindrical geometry and substrate material are considered to be the same as in Fig. 7. There are two different physical phenomena taking place for even and odd transverse current distributions. When the lines are tightly

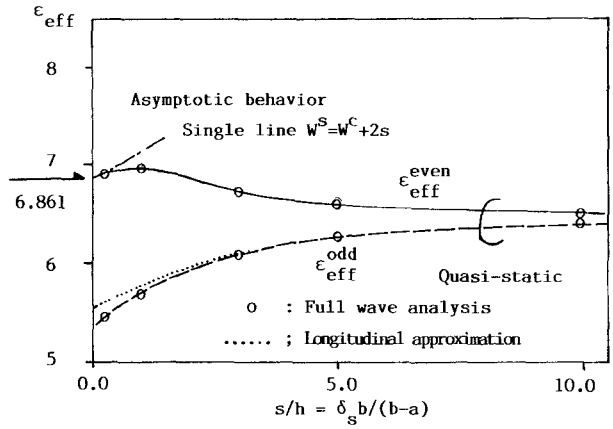

Fig. 7. Low-frequency coupled microstrip line properties as a function of line separation. $R = a/b = 0.9$, $W/h = \delta_w b/(b-a) = 1.0$, $\epsilon_r = 9.6$, and $k_0 b = 0.1$.

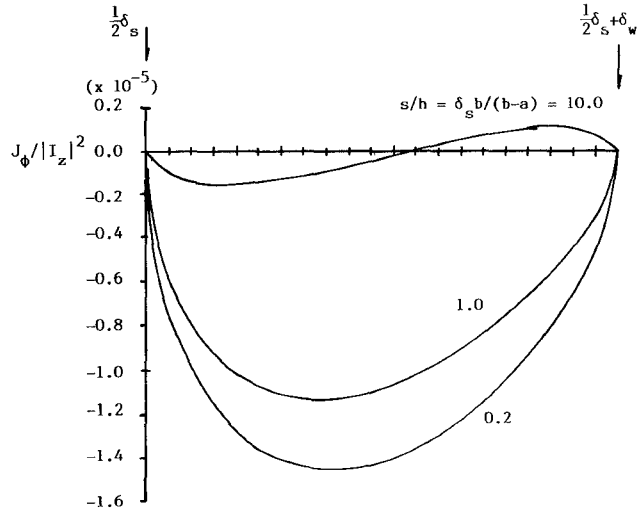

Fig. 8. Odd-mode current behavior as a function of line separation. $R = 0.9$, $\epsilon_r = 9.6$, $W/h = 1.0$, and $k_0 b = 0.1$. Number of base functions: longitudinal current - 20; transverse current - 20.

TABLE I
NUMERICAL COMPARISON OF QUASI-STATIC, FULL-WAVE, AND LONGITUDINAL APPROXIMATION

Odd mode			
s/h	Quasi-static (Appendix I)	Full wave* (Present theory)	Longitudinal** approximation
0.2	5.485 31.65	5.486 (.02%) 31.67 (.06%)	5.598 (2.1%) 49.84 (57.%)
1.0	5.722 43.72	5.722 (****) 43.76 (.09%)	5.774 (.91%) 48.44 (11.%)
10.0	6.369 50.97	6.372 (.05%) 51.01 (.08%)	6.376 (.11%) 50.50 (.92%)

Even mode			
s/h	Quasi-static (Appendix I)	Full wave* (Present theory)	Longitudinal** approximation
0.2	6.921 66.46	6.926 (.07%) 66.55 (.14%)	6.943 (.32%) 66.46 (****)

$R = 0.9$, $\epsilon_r = 9.6$, $k_0 b = 0.1$ (*,**), and $W/h = \delta_w b/(b-a) = 1.0$.
*$N = 20$ for both longitudinal and transverse current.
**$N = 20$ for longitudinal current and $N = 0$ for transverse current.

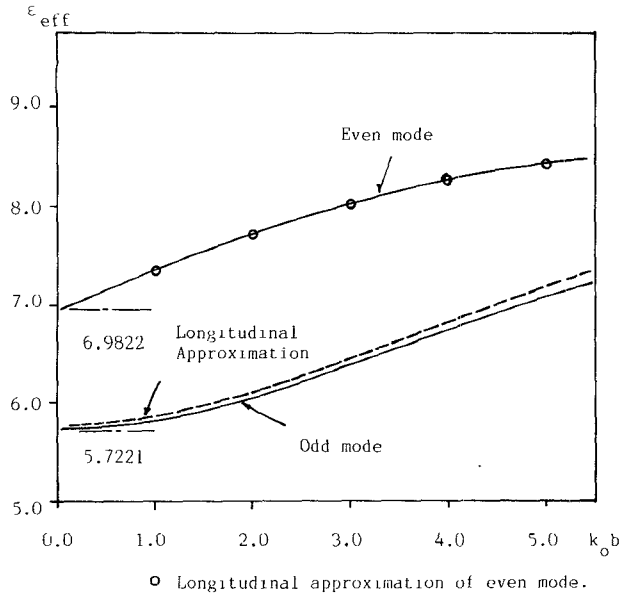

Fig. 9. Frequency-dependent even/odd-mode effective dielectric constant. $R = 0.9$, $\epsilon_r = 9.6$, $W/h = 1.0$, and $s/h = 1.0$.

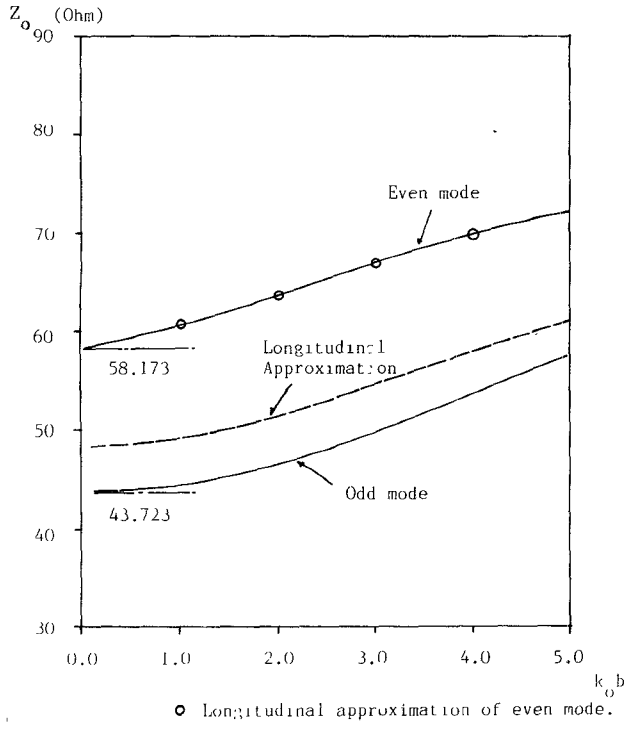

Fig. 10. Frequency-dependent even/odd-mode characteristic impedance. $R = 0.9$, $\epsilon_r = 9.6$, $W/h = 1.0$, and $s/h = 1.0$.

coupled, the odd-mode transverse electric field component becomes very strong between the lines, so that the transverse current flow is dominated by this field. On the other hand, the even-mode transverse current flow is dominated by the two lines merging together as a one line system when the separation is small. Consequently, the even-mode transverse current also shows a behavior similar to that observed for the odd mode. When the separation gets wider, the transverse current starts to show an antisymmetric behavior, since there is not enough coupling to affect the transverse current component. A numerical comparison of these cases is also presented in Table I.

Finally, the last two figures show the frequency-dependent characteristics of the coupled microstrip lines. Here we consider $R = 0.9$, $W/h = 1.0$, and $s/h = 1.0$ for alumina. It can be seen that the longitudinal current approximation agrees quite well for the even mode. However, the odd mode shows a significant difference, especially for the characteristic impedance.

IV. Conclusions

The frequency-dependent characteristics for single and coupled microstrip lines on a coated cylinder are obtained with an exact dyadic Green's function formulation. When the numerical procedure is carefully developed, all the physical phenomena are observed and the transverse electric field and current are found to be extremely significant, especially for the odd-mode case. The algorithm for computing the cylindrical substrate geometry Green's function is proven to be very accurate and efficient.

Appendix

The quasi-static formulation is presented here since the numerical comparison with the frequency-dependent solution has relied on this model.

The potential Green's function for the single-layer problem can be readily obtained as [6]

$$g(b,\phi) = \frac{1}{2\pi\epsilon_0}\left[\frac{1}{\epsilon_r}\log(1/R) + 2\sum_{m=1}^{\infty}\frac{\cos\{m(\phi-\phi')\}}{m\{1+\epsilon_r\coth(m\log(1/R))\}}\right]. \quad \text{(A1)}$$

The charge distribution is approximated by a set of pulse basis functions with a subsegment width of D and the even/odd mode condition is imposed on the problem. When the Galerkin method is applied, we obtain the system of equations as $[V_n] = [Z_{nn'}][c_{n'}]$. Since the potential on the strip is constant, $V_n = 1$, the impedance matrix element is derived in the form

$$Z_{nn'} = \frac{8}{\pi\epsilon_0 D}\left[p\frac{D^2}{8\epsilon_r}\log(1/R) + \sum_{m=1}^{\infty}\frac{\begin{matrix}\cos\\ \sin\end{matrix}(m\phi_n)\begin{matrix}\cos\\ \sin\end{matrix}(m\phi_{n'})\sin^2\left(\frac{mD}{2}\right)}{m^3\{1+\epsilon_r\coth(m\log(1/R))\}}\right] \quad \text{(A2)}$$

with

$$p = \begin{cases}1\text{: even mode}\\ 0\text{: odd mode.}\end{cases}$$

Here the even mode corresponds to the upper and the odd mode to the lower case. The closed-form formulation is obtained by observing that $\coth(m\log(1/R)) \sim 1$ as $R \to 1$. The same technique is also applied to the frequency-dependent model. We have determined that when R is

close to unity, the closed-form formulation requires a relatively large number of correction terms. This is also true for the frequency-dependent model since the functional behavior for large order is expected to be the same as that for the quasi-static case. The convergence rate of the above summation relies on the value of D. When D is small, it can be observed that the convergence rate is very slow, and for the extreme case of $D = 0$ the series diverges. This is the case of singular solution, when the source is an impulse source and the system function is white noise.

References

[1] N. G. Alexopoulos, P. L. E. Uslenghi, and N. K. Uzunoglu, "Microstrip dipole on cylindrical substrates," *Electromagnetics*, vol. 3, nos. 3–4, pp. 311–326, July–Dec. 1983.

[2] L-R. Zeng and Y. Wang, "Accurate solutions of elliptical and cylindrical striplines and microstrip lines," *IEEE Trans. Microwave Theory Tech.*, vol. MTT-34, pp. 259–265, Feb. 1986.

[3] S. B. Fonseca and A. J. Giarola, "Analysis of microstrip wraparound antennas using dyadic Green's functions," *IEEE Trans. Antennas Propagat.*, vol. AP-31, no. 2, pp. 248–253, Mar. 1983.

[4] A. Nakatani and N. G. Alexopoulos, "Modeling microstrip circuits and microstrip antennas on cylindrical substrates," in *APS-Symp Dig.*, vol. 1, June 1986, pp. 439–442.

[5] A. Nakatani, N. G. Alexopoulos, N. K. Uzunoglu, and P. L. E. Uslenghi, "Accurate Green's function computation for printed circuit antennas on cylindrical substrates," *Electromagnetics*, vol. 6, no. 3, July–Sept., 1986.

[6] N. G. Alexopoulos and A. Nakatani, "Cylindrical substrate microstrip line characterization," *IEEE Trans. Microwave Theory Tech.*, vol. MTT-35, pp. 843–849, Sept. 1987.

[7] M. Kobayashi and F. Ando, "Dispersive characteristics of open microstrip lines," *IEEE Trans. Microwave Theory Tech.*, vol. MTT-35, pp. 101–105, Feb. 1987.

[8] M. Kobayashi, "Longitudinal and transverse current distribution on microstriplines and their closed-form expression," *IEEE Trans. Microwave Theory Tech.*, vol. MTT-33, pp. 784–788, Sept. 1985.

[9] E. J. Delinger, "A frequency dependent solution for microstrip transmission lines," *IEEE Trans. Microwave Theory Tech.*, vol. MTT-19, pp. 30–39, Jan. 1971.

[10] T. Itoh and R. Mittra, "Spectral-domain approach for calculating the dispersion characteristics of microstrip lines," *IEEE Trans. Microwave Theory Tech.*, vol. MTT-21, pp. 496–499, July 1973.

[11] K. C. Gupta, R. Garg, and I. J. Bahl, *Microstrip Lines and Slotlines*. Norwood, MA: Artech House, 1979.

[12] E. Costamagna, "Characteristic impedance of microstrip lines," *IEEE Trans Microwave Theory Tech.*, vol. MTT-35, pp. 35–40, Jan. 1987.

[13] M. Abramowitz and I. A. Stegun, *Handbook of Mathematical Functions*. New York: Dover, 1964.

[14] I. S. Gradshteyn and I. M. Ryzhik, *Table of Integrals, Series, and Products*. New York: Academic Press, 1980.

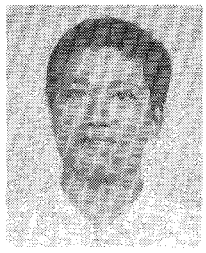

Akifumi Nakatani (S'81) was born in Tokyo, Japan, on February 10, 1956. He received the B.S.E.E. degree from Iwate University, Iwate, Japan, in 1979 and the M.S.E.E. degree from Oregon State University in 1981. He is currently studying at the University of California, Los Angeles, for the Ph.D. degree. His research interests include the computer-aided analysis and design of microwave and millimeter-wave components and printed circuits on curved geometries.

Nicólaos G. Alexópoulos (S'68–M'69–SM'82–F'87) was born in Athens, Greece, in 1942. He graduated from the 8th Gymnasium of Athens and subsequently obtained the B.S.E.E., M.S.E.E., and Ph.D. degrees from the University of Michigan, Ann Arbor, in 1964, 1967, and 1968, respectively.

He is currently a Professor in the Department of Electrical Engineering, University of California, Los Angeles, Associate Dean of the School of Engineering and Applied Science, and a Consultant with Northrop Corporation's Advanced Systems Division. His current research interests are in electromagnetic theory as it applies to the modeling of integrated-circuit components and printed circuit antennas for microwave and millimeter-wave applications, substrate materials and their effect on integrated-circuit structures and printed antennas, integrated-circuit antenna arrays, and antenna scattering studies. He is the Associate Editor of the *Electromagnetics Journal* and *Alta Frequenza*, and he is on the Editorial Boards of the IEEE TRANSACTIONS ON MICROWAVE THEORY AND TECHNIQUES and the *International Journal on Electromagnetic Theory*.